Flow and Thermal Field Measurements in a Combustor Simulator Relevant to a Gas Turbine Aeroengine

S. S. Vakil

K. A. Thole

Mechanical Engineering Department,
Virginia Polytechnic Institute and State University,
Blacksburg, VA 24061

The current demands for high performance gas turbine engines can be reached by raising combustion temperatures to increase power output. Predicting the performance of a combustor is quite challenging, particularly the turbulence levels that are generated as a result of injection from high momentum dilution jets. Prior to predicting reactions in a combustor, it is imperative that these turbulence levels can be accurately predicted. The measurements presented in this paper are of flow and thermal fields produced in a large-scale combustor simulator, which is representative of an aeroengine. Three-component laser Doppler velocimeter measurements were made to quantify the velocity field while a rake of thermocouples was used to quantify the thermal field. The results indicate large penetration depths for the high momentum dilution jets, which result in a highly turbulent flow field. As these dilution jets interact with the mainstream flow, kidney-shaped thermal fields result due to counter-rotating vortices that develop. [DOI: 10.1115/1.1806455]

Introduction

The flow and thermal fields in a combustor are one of the most complex occurrences in a gas turbine engine and subsequently the most difficult to predict. Typical gas turbine engine combustors for aeroengines have a chamber with a flow area defined by an annulus containing evenly spaced fuel-injection nozzles. Annular combustion chambers have the advantage of requiring less space and weight than cannular chambers, for example, but have the disadvantage of being difficult to obtain both a uniform air-fuel distribution and exit condition.

To evaluate the flow and thermal fields that occur in a typical combustor of an aeroengine and to further our computational predictive methods, a large-scale facility was developed to simulate prototypical combustor flows. Although the simulation presented in this paper has not included the reacting flow thereby not including such effects as the heat release due to combustion, it is important to recognize that we should begin by determining whether we can experimentally and computationally simulate the nonreacting flow field. The heat release, for example, will depend upon the mixing characteristics of the dilution jets. If the dilution jets cannot be accurately simulated under the nonreacting conditions, it would be difficult to simulate the reacting flow field. In particular, predicting the turbulent flow fields for high momentum, normal jets (dilution jets) in crossflow is very difficult. For the design of the facility reported in this paper, nonuniformities in both the span (radial) and pitch (circumferential) directions exiting the combustor have been simulated through the use of cooled combustor walls, ensuring representative near-wall flows, and dilution jets, ensuring representative mainstream flows with high levels of turbulence.

The objective for the work reported in this paper was to quantify the flow and thermal field conditions for a prototypical combustor design that is nonreacting. Predictions of highly separated jets are relevant to that occurring in most aeroengine combustor designs. The dataset reported in this paper can be used for direct comparisons to computational fluid dynamics simulations for the geometry provided. Most often the turbulence produced is underpredicted with standard two-equation turbulence models (typically used in industry). This underprediction results in two concerns. First, the mean flow field will be predicted to have much stronger secondary flows (counter-rotating vortices from the dilution jets) than are actually present. Also, the trajectory of the dilution jets will not be accurately predicted, which make it impossible to track the mixing zones. Second, the mixing characteristics will be underpredicted resulting in a misprediction of the temperature profile entering the turbine. The data provided in this paper gives the community an opportunity to compare their predictions of the flow and thermal field in a scaled-up combustor prior to predicting the more complicated case with reacting flow. After describing the development of the combustor simulator facility, this paper describes the experimentally measured flow and thermal fields.

Relevant Past Studies

Many experimental studies have been reported in the open literature documenting both experimental and computational data for model combustor flows. The large number prevents a full discussion of all of the results in our paper. None of these studies, however, have provided spatially resolved mean and turbulent flow fields as well as thermal fields for a combustor simulator that includes two rows of staggered dilution jets, and a film-cooled liner wall, which are all upstream of a stator vane sector. The combustor geometry reported in our paper is modeled after a modern aeroengine design in which both liner-cooling and dilution jets are simulated. While a complete summary of the literature documenting combustor-type measurements can be found in Barringer [1], only a few relevant studies will be discussed in our paper.

Since the work presented in our paper is for a nonreacting combustor, it is necessary to address any differences that may occur between the measurements we are reporting and those for a reacting combustor. Zimmerman [2] conducted one of the first investigations that measured combustor-generated turbulence at the exit of a can-type combustor. Turbulence levels, based on local velocities, ranged between 7% (at idle conditions) and 10% (at takeoff

Contributed by the International Gas Turbine Institute (IGTI) of THE AMERICAN SOCIETY OF MECHANICAL ENGINEERS for publication in the ASME JOURNAL OF ENGINEERING FOR GAS TURBINES AND POWER. Paper presented at the International Gas Turbine and Aeroengine Congress and Exhibition, Atlanta, GA, June 16–19, 2003, Paper No. 2003-GT-38254. Manuscript received by IGTI, October 2002, final revision, March 2003. Associate Editor: H. R. Simmons.

conditions). The measurements indicated the same turbulence levels independent of whether combustion took place. Goldstein et al. [3] performed LDV measurements at the exit of two can-type combustors with and without combustion to determine its effect on the velocity and turbulence profiles at the combustor exit. They reported turbulence levels, based upon local velocities, ranging between $25\% < Tu < 35\%$ without reactions and $15\% < Tu < 25\%$ with reactions. The dependence of the turbulence levels upon reactions contradicts the measurements performed by Zimmerman [2] and Moss [4], who showed no dependence.

Cameron et al. [5] conducted detailed spatial mappings of velocity and temperature in the nonreacting and reacting environment of a model gas turbine combustor with a dilution jet, similar to that of our configuration. They concluded that a strong on-axis recirculation zone located upstream of the dilution jets was present in the nonreacting case, but was dissipated in the reacting case. The combustor exit turbulence levels were 25% for the reaction case, but no data was available for the nonreacting case.

While some differences may occur, it is important to recognize data is needed to allow for computational benchmarking. A number of studies have demonstrated the shortfalls of computational predictions for combustor-type flows in that there is an underprediction of the turbulence levels. Predicting the turbulence levels is relatively important if accurate mixing predictions are desired. Gulati et al. [6] measured the mean and rms temperatures at the exit plane of a full-scale, ten-cup, double annular research combustor. Their results indicated that the dilution air had a significant affect on the mean and rms temperature profiles. As the outer row of dilution air was increased, the jets pushed the combustion zone toward the inner liner and increased the peak temperature. While these trends were predicted well by computational models using the standard k-ϵ turbulence model, the model consistently underpredicted the fluctuations at the exit. This trend of underpredicting the turbulence levels is in agreement with the findings of Holdeman [7] and Stitzel [8].

Malecki et al. [9] reported results using the standard k-ϵ turbulence model with wall function near-wall modeling. To overcome the low turbulence level predictions, reduced Schmidt numbers (Sc) were used to compensate for the low turbulence levels in the mixing of the product species. Using this scheme, good agreement was achieved between circumferentially averaged exit temperature profiles from the test rig data and the computational predictions.

Several studies have been reported that discuss the various effects of different combustor features. In the majority of these studies, the dictating features of a combustor flow field are governed by the presence of high momentum dilution jets. Goebel et al. [10], for example, measured velocity, turbulence, and temperature profiles downstream of a reacting small-scale combustor. They found that with an appreciable swirl velocity, the dilution jets acted to disrupt the swirl and actually reduce the turbulence levels. Without swirl and at low swirl velocities, the transverse dilution jets increased the turbulence levels. Stevens and Carotte [11] also experimentally investigated the combustor dilution zone and jet development by focusing on the downstream thermal field in a nonreacting, annular combustor simulator. Their measurements revealed each jet exhibited a kidney-shaped contour, which is a characteristic of jets-in-cross-flow. Liou and Wu [12] made measurements for a nonreacting combustor that consisted of a rectangular duct with two opposing side jets. One finding from the study was that the turbulence was inhomogeneous and anisotropic throughout most regions of the combustor simulator.

Holdeman [7] simulated a nonreacting gas turbine combustion chamber by conducting computations and experiments on the mixing of single, double, and opposed rows of dilution jets with an isothermal or variable temperature mainstream in a confined subsonic cross flow. The principle finding from the investigation was that the momentum flux ratio of the jets dictated the exit velocity and temperature profiles. The results from the cases involving opposed rows of jets revealed that for in-line jets the two streams mixed very rapidly and that the effective mixing height was half the duct height for equal momentum flux ratios on both sides.

In summary, comparing the results from the studies presented in the literature indicate that there are some differences for a reacting and nonreacting flow near the primary zone. Most studies have indicated the importance of simulating the dilution jets. The turbulence levels at the combustor exit that were reported for the studies with reaction, were very similar to those found in the studies without reaction. There was good agreement between computations, which used some form of a two-equation turbulence model, and experiments in predicting dilution jet penetration and combustor exit temperature profiles. The computational models, however, do not have the ability to accurately predict the turbulent mixing that occurs in the dilution zone. As a result of this inability, we believe that it is important to provide data documenting the flow in a combustor environment that is nonreacting. This data provides the first test for computational predictions.

Experimental Facilities

The development of the combustor simulator used in our study was previously described by Barringer et al. [13]. The geometric scaling factor for the combustor was $9\times$, which allows for good measurement resolution in the experiments. This scaling factor was matched to that of a linear turbine vane cascade that was pre-existing. Note that the turbine vane is not the focus of this paper. Measurements that are presented in this paper include mean and turbulent velocities as well as mean temperatures.

Experimental Facilities. Other than performing the measurements in an actual operating engine, it is not feasible to provide a measurement environment with representative turbine engine conditions. In designing this combustor simulator, the parameters that were chosen for a prototypical combustor for aircraft applications included the following: (i) a nondimensional acceleration parameter through the combustor; (ii) a combustor exit velocity that ensured the needed inlet Reynolds number for the downstream turbine section; (iii) coolant-to-mainstream momentum flux ratios of the liner cooling holes and the dilution holes; and (iv) scaled geometric features of a combustor including the film-cooling staggered hole pattern and dilution hole size and placement. Note that the parameters for the prototypical engine combustor are for actual running (hot) operating conditions. The air loading parameter (ALP defined in the nomenclature) for the wind tunnel design was 0.40×10^{-4}.

Figure 1 illustrates the wind tunnel containing the combustor simulator and turbine vane test sections. Downstream of a primary heat exchanger is a transition section that divides the flow into three channels that include a heated primary channel, representing the main gas path (center arrows), and two symmetric secondary channels (outer arrows), representing the coolant flow path. Within the transition section of the primary channel, the flow immediately passes through a perforated plate that provides the necessary pressure drop to control the flow splits between the primary and secondary passages. At a distance 2 m downstream of the perforated plate, the flow passes through a bank of heaters followed by a series of screens and flow straighteners. The heater section comprises three individually controlled banks of electrically powered, finned bars supplying a maximum total heat addition of 55 kW. Downstream of the flow straighteners, the heated primary flow enters the combustor simulator. In the combustor simulator, secondary coolant flow is injected into the primary flow passage through cooling panels for the combustor liner and through dilution holes. In addition, the flow is accelerated prior to entering the turbine section. In addition to heat being rejected from the primary heat exchanger, the flow in the secondary passages must pass through a second heat exchanger to further reduce

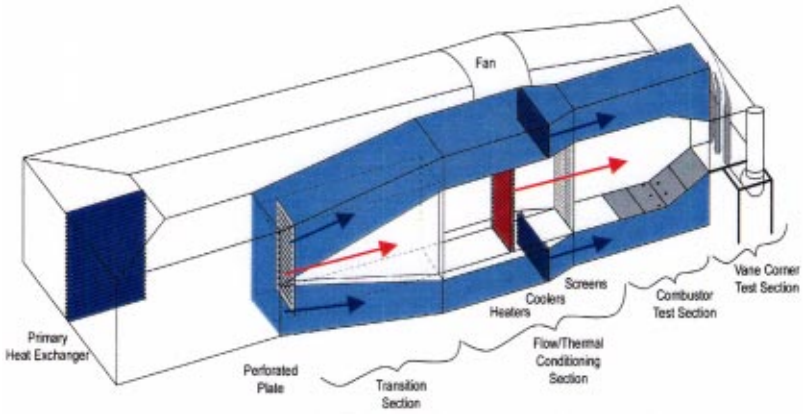

Fig. 1 Illustration of the wind tunnel facility used for the combustor simulator experiments

the coolant flow temperature. The flow in the secondary passages is then directed into a large plenum that supplies combustor liner coolant and dilution flow.

The cooling hole pattern in the panels is illustrated in Figs. 2(*a*)–2(*b*). To ensure representative coolant flow splits among the four liner panels and dilution rows, separate supply chambers with adjustable shutters were used. The mass flow exiting the film-cooling holes was set by applying the appropriate pressure ratio between the supply plenum and the exit static pressure. Using previously documented discharge coefficients (Barringer et al. [13]) the mass flows through the panels were determined. The mass flows exiting the dilution holes were set by directly measuring the velocity through the use of a pitot probe installed at the exit of the dilution hole.

The combustor simulator begins at the start of the first panel, as illustrated in Fig. 2(*a*). The cross-sectional area of the simulator at this location is 1 m in height (H_{in}) and 1.1 m in width (W). At the exit of the simulator, the cross-sectional area is 0.55 m in height and remained 1.1 m in width, giving an area ratio of 1.8. The width was to allow for a span that was slightly greater than a turbine sector while the height was matched to that of the radial extent of a first vane.

The liners for the combustor simulator were a streamwise series of four film-cooled panels that started 2.7 vane chords (1.6 m) upstream of the turbine test section. The first two panel lengths were 39 and 41 cm while the third and fourth panels were 37 and 43 cm. The panels extended across the full width of the test section, which was slightly greater than a scaled turbine sector. The

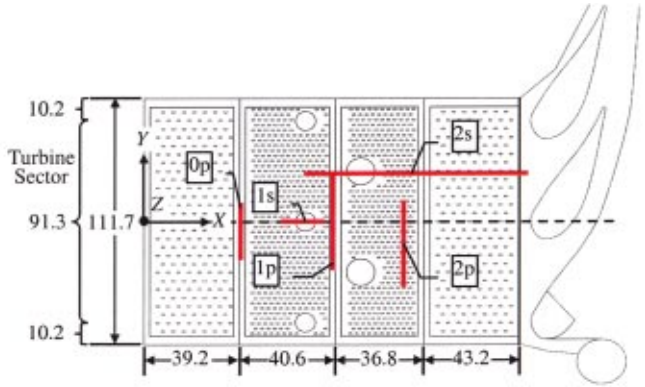

(a)

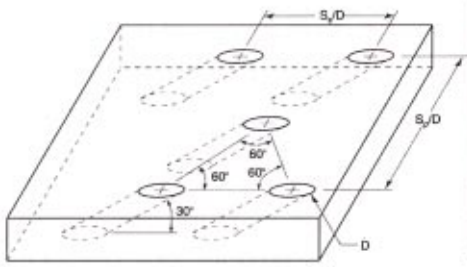

	S_y/D	S_x/D
Panel 1	10.1	5.8
Panel 2	6.1	3.5
Panel 3	6.1	3.5
Panel 4	10.1	5.8
Dilution 1	60 (5.4 D_1)	90 (8.1 D_1)
Dilution 2	60 (3.8 D_2)	121 (7.6 D_2)

(b)

Fig. 2 (*a*) Layout and measurements planes for the combustor simulator (dimensions in cm). (*b*) Illustration and description of cooling hole arrangement for liners.

Table 1 Summary of Coolant Flow Conditions

	% Mass Flow Addition Based on Local Flow Rate	Momentum Flux Ratio Based on Local Mass-Averaged Velocity	Mass Flux Ratio Based on Local Mass-Averaged Velocity	Density Ratio Based on Ups tream Flow Conditions	Ratio of Mass-Averaged Velocity to Inlet Velocity
Panel 1	2.6	9	3.2	1.12	1
Panel 2	6.3	9	3.2	1.12	1
Panel 3	5.4	9	3.2	1.12	1.6
Panel 4	2.2	9	3.2	1.12	2.7
Dilution 1	18.5	128	12	1.12	1
Dilution 2	12.5	32	6	1.12	1.6

first two panels were flat to maintain a constant cross-sectional area while the following two panels were inclined at 15.7 deg to give the required area contraction. The panels were constructed of 1.27 cm thick urethane foam with a low thermal conductivity ($k = 0.037$ W/mK) to allow for adiabatic surface temperature measurements. The dense matrices of film-cooling and dilution holes were cut into the urethane foam using a water jet.

One parameter that is not representative is the coolant-to-mainstream density ratios, which are typically quite high. Typical operating conditions consisted of a flow temperature just downstream of the heater of nominally 50°C and a coolant flow temperature of 20°C. As the coolant flow progressed downstream through the secondary flow channel, there was a small increase in the fluid temperature of nominally 1°C. Although the density ratios were not matched, the jet-to-mainstream momentum flux ratios and percentage of mass flow addition by both the film-cooling and dilution holes were representative. The momentum flux ratio is the parameter that most affects mixing characteristics of jets in cross-flow at high momentum flux ratios. The cooling hole patterns, shown in Fig. 2(*b*), were configured in equilateral triangles and spaced evenly across the panel surface. The diameter of the cooling holes was 0.76 cm, giving an $L/D = 3.3$.

The dilution hole diameters were designed to insure the percent mass addition of the dilution fluid and coolant-to-mainstream momentum flux ratios were representative of that in an engine. This first row of dilution holes has three holes evenly spaced with the center hole being aligned with the center of the simulator (and also the vane stagnation). This first row is located at 43% of the combustor length (0.67 m) downstream of the start of the panels. The dilution holes in the first row have a diameter that is 8.5 cm. The second row of dilution holes was located on the third panel at 57% of combustor length (0.90 m) downstream of the start of the panels. The second row of dilution holes contained two holes having a diameter of 12.1 cm. The two dilution holes were staggered with respect to the first row of holes. The supply chamber for the dilution flow was required to be some distance from the hole exits giving an L/D ratio of 1.5 for both rows. The combustor simulator is symmetric about the vertical mid-span meaning that for each row the dilution holes were aligned with one another in the pitchwise and streamwise directions.

As indicated for the operating conditions of the results reported in this paper in Table 1, 45% of the flow is directed through the primary passage of the combustor simulator while 55% of the flow is directed through the secondary coolant passages for the liner coolant and dilution holes. Of the total cooling flow 36% is injected through the film-cooling holes and 64% is injected through the dilution holes.

Instrumentation and Measurement Uncertainty. Thermocouples were used in monitoring inlet and coolant temperatures as well as taking the thermal fields within the combustor. All of the temperature measurements were made using 30-gauge, type E thermocouples that were connected to a data acquisition system through 20-gauge thermocouple extension wire. All of the thermocouples used in this study were made using an argon-gas thermocouple welder that resulted in spherical beads ranging in diameter from a minimum of approximately 0.8 mm to a maximum of ~1 mm. The thermal fields were taken using a 21 probe thermocouple rake. The rake spanned a total distance of 10.2 cm with thermocouples evenly spaced every 5.1 mm. Each thermocouple probe on the rake consisted of a 5.1 cm long, 2.5 mm outer diameter aluminum casing that encapsulated the thermocouple wire. The approximate flow blockage was shown to have no effect on the measured thermal field. Each thermocouple bead is fixed approximately 6.4 mm from the end aluminum shaft in order to minimize heat conduction effects from the aluminum rod to the thermocouple.

Velocities were measured using a two- and three-component laser Doppler velocimeter (LDV). The flow was seeded with olive oil particles that were nominally 1 μm in diameter. The probability of obtaining a sample was proportional to the speed of the flow; therefore, statistical particle bias corrections were applied to the data by weighting each individual sample based on the residence time of a particle in the probe volume.

In taking flow plane measurements that were aligned with the flow direction, a single fiber-optic LDV probe capable of measuring two components was used. This setup used a 350 mm focusing lens without a beam expander and had a measurement volume of 90 μm in diameter and 1.3 mm in length. The plane was acquired with the probe perpendicular to the outer wall surface. This allowed for the direct measurement of the local streamwise velocity component, u. However, in order to take measurements near the surface of the liner panel, the probe was slightly tilted at 7 deg, whereby there was little effect on the true vertical component measurements.

For the measurements taken in the cross-stream direction where three-component velocity measurements were made, two separate fiber optic probes were used. To allow the measurement volume of the probes to reach the mid-pitch of the combustor simulator, a 2.6 magnification beam expander along with a 750 mm focusing lens were used. With the use of the beam expander, the measurement volume was 73 μm in diameter and 1.3 mm in length. Using these two probes, the measurements were conducted through a nonorthogonal setup requiring the velocity components to be transformed into the true components. Furthermore, as with the single LDV probe measurements, a tilt was applied to both probes to allow for near-wall measurements. To ensure a single beam crossing, both probes were turned 13 deg toward each other off the cross-stream direction while the vertical tilt angle was set to 7 deg.

In order to compare the day to day repeatability of the test conditions and ensure that the correct velocity transformations were made, the two- and three-component LDV data were compared where streamwise and spanwise measurement planes overlapped. This data is shown in Fig. 3 whereby the measurement times spanned several weeks. The location of this data was just downstream of the first dilution row and in the spanwise middle of

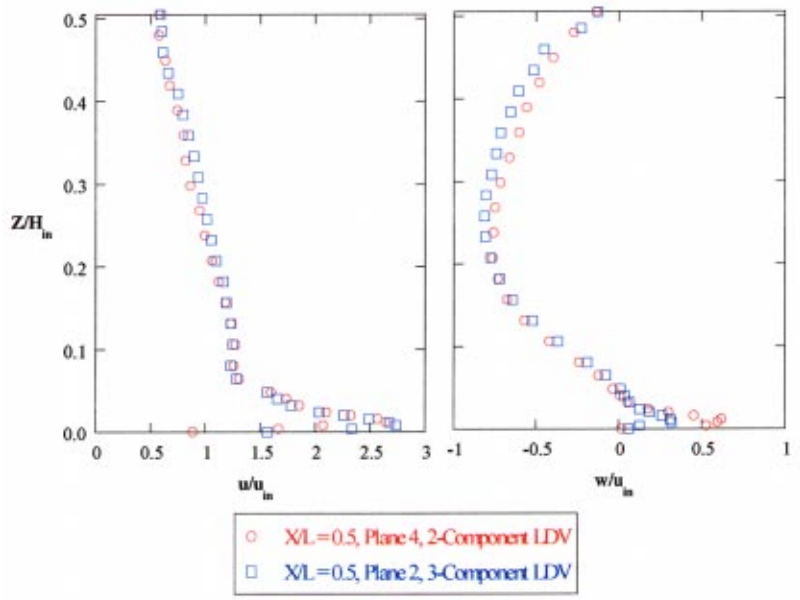

Fig. 3 Comparisons of two and three-component LDV profiles measured independently in an overlap location just downstream of the first row of dilution

the outer second row dilution hole. This data indicates consistency of the velocity transformations that were applied to the data as well as the repeatability of the test conditions.

The nominal sampling time for each measurement location was 40 s whereby 15,000 data points were acquired for each component. For the longer 750 mm focusing lens most measurement locations had an average sampling time of approximately 100 s for the same sample size.

The partial derivative and sequential perturbation methods, described by Moffat [14], were used to estimate the uncertainties of the measured values. Precision uncertainties were calculated based on a 95% confidence interval. The precision uncertainty for the streamwise rms velocities was 2.6% while the bias uncertainty for the mean velocity measurements was 1%. The bias and precision uncertainties on the thermal field values, was ± 0.04, giving an uncertainty of 4.5% at $\theta=0.9$ and 12.6% at $\theta=0.3$.

Measured Flow and Thermal Field Results

The measurements made in this study were taken at a number of different locations within the combustor simulator, as shown in Fig. 2(*a*). These locations were chosen to illustrate the different flow conditions that can occur throughout the combustor and include the following: (i) downstream of the first liner whereby film-cooling holes are present (plane $0p$); (ii) downstream of the first row of dilution holes whereby the jets are being injected at a high momentum flux ratio (planes $1p$ and $1s$); and (iii) downstream of the second row of dilution holes whereby the jets are being injected from a liner wall that is contracting (planes $2p$ and $2s$). The flow conditions that were set are summarized in Table 1 for each of the panel and dilution flows. Note that two different film-cooling flows were studied for the first panel ($I=3$ and 9), but for the remainder of the measurements an $I=9$ condition was set for this panel.

Liner With Multiple Rows of Film-Cooling Holes. Thermal field measurements were performed just downstream of the first cooling panel in plane $0p$ for two different flow conditions. The measurement location was at $X/L=0.24$, which is two film-cooling hole diameters downstream of the last row of cooling holes ($X/d=2$) in panel one. The average momentum flux ratios for this panel were set to either $I=3$ or 9, giving an average mass flux ratio for the panels of $M=1.8$ and 3.2, respectively. Fifteen rows of staggered film-cooling holes were present in this panel

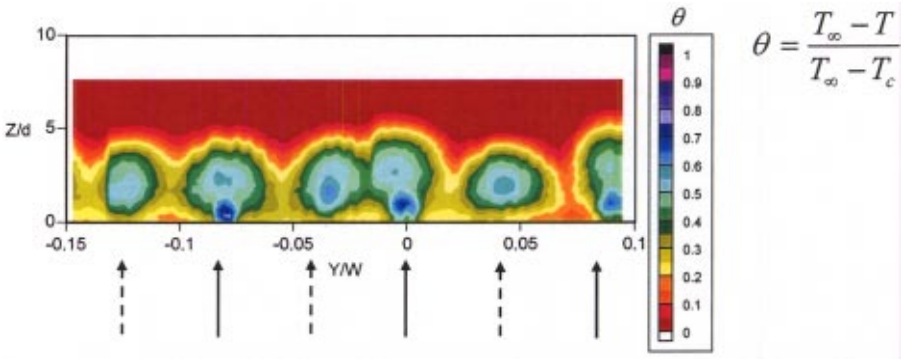

Fig. 4 Film-cooling thermal field measurements in plane $0p$ with an average liner flow of $I=3$, $DR=1.1$

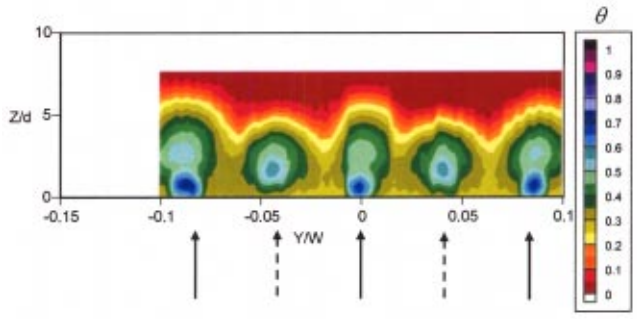

Fig. 5 Film-cooling thermal field measurements in plane 0*p* with an average liner flow of *I*=9, *DR*=1.1

with the hole spacing as that indicated in Fig. 2(*b*). While these measurements were conducted, the flow condition for the remaining liner panels was set at the same condition as the first panel ($I=3$ or 9). Figures 4 and 5 show the measured thermal fields for the two blowing conditions. The solid arrows represent the location of the last row of film-cooling holes while the dashed arrows represent the pitch location of the previous row of film-cooling holes. As can be seen by the thermal field measurements, the jets are periodic in the pitch direction across the panel.

Figures 4 and 5 indicate a cooler jet for the row of jets closest to the measurement plane (solid arrows) as compared with the jets of the previous row (dashed arrows). For both flow conditions, the peak temperature contour representing the coolest fluid is located away from the wall. A separated jet condition is expected given the high momentum flux ratio conditions for both cases. The thermal field contours for the row of cooling holes closest to the measurement plane indicate a double-peak with the second peak being at a slightly warmer temperature ($\theta=0.5$) than the primary peak ($\theta=0.7$). The second peak is located just above the coldest peak and is a remnant of the upstream cooling jet at the same pitchwise alignment. Interestingly, the contour levels for the dashed arrows (upstream row) do not have this double peak, which indicates that given enough streamwise distance the streamwise jets merge into one cooler core.

Although the conditions through the holes differ by a large amount of cooling flow, the core of the jets closest to the measurement plane (coldest contour) is nominally at the same temperature level at this location ($\theta=0.7$) for both blowing ratios. There are two real differences between these two cases. First, the penetration depth for the $I=9$ case appears to be greater than the $I=3$ case. Second, and more importantly, the fluid temperature between the jets near the wall appears to be cooler for the $I=9$ case ($0.25<\theta<0.35$) as compared with the $I=3$ case ($0.15<\theta<0.2$).

Downstream of the First Row of Dilution Holes. The thermal field measured in the streamwise direction through the first row of dilution jets is shown in Fig. 6. Recall at this location in the combustor simulator, the cross-sectional area of the simulator is the same as that of the entrance. The spanwise distance (Z) is normalized by this height (H_{in}). The momentum flux ratio for this large dilution jet is $I=128$ while the mass flux ratio is $M=12$.

The contours in Fig. 6 indicate a penetration distance that is approximately 18% of the height before the jet trajectory is bent over by the mainstream flow. Upstream of the jet injection, there is a relatively thick film-cooling layer that is being transported into the free stream by the dilution jet. It is also clear that the temperature gradients are quite high at the jet-mainstream interface near the jet injection, while farther away from the wall the temperature contours are spreading due to the turbulent mixing. The penetration depth of these dilution jets does not extend to the centerline, which is quite probably a result of the opposing jets that are aligned in the pitchwise and streamwise locations.

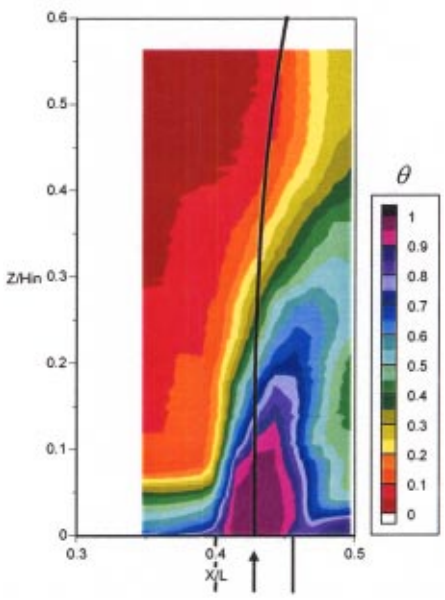

Fig. 6 Thermal field contours in a streamwise plane through a first row dilution hole (plane 1*s*) with Lefebvre's [15] jet penetration correlation

The solid line shown in Fig. 6 indicates the penetration distance predicted by the correlation given by Lefebvre [15]. The correlation overpredicts the trajectory of the jet and underpredicts the bending of the jet. One plausible reason for the misprediction may be due to the fact that there is an opposing jet and that these dilution jets are at very high momentum ratios ($I=128$).

Figure 7 shows the measured thermal field for a plane that extends in the pitchwise direction downstream of the first row of dilution jets at a location that is two film-cooling hole diameters downstream of the last row of cooling holes in the second liner. This location is 1.3 hole diameters ($X=1.3D_1$) downstream of the dilution hole whereby this distance is measured from the hole centerline. This larger plane was taken to illustrate the pitchwise symmetry of the dilution flow. These thermal fields indicate that the coolant from the dilution jets has been transported to a region slightly offset from the center of the two lobes of the kidney-shaped vortex. It is important to recognize that the distance be-

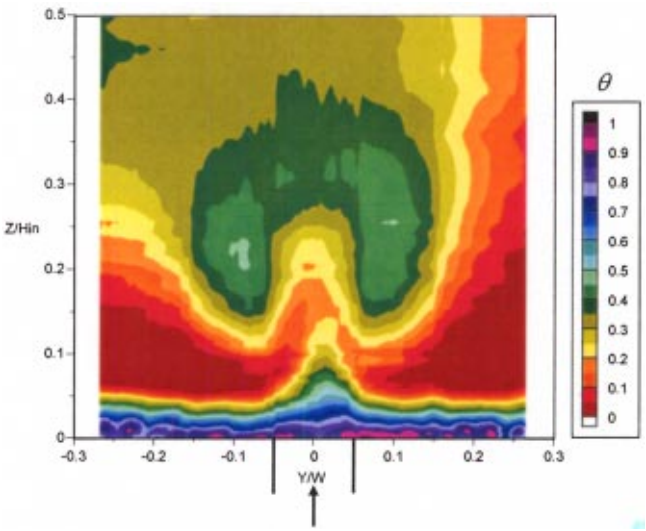

Fig. 7 Thermal field contours in plane 1*p*

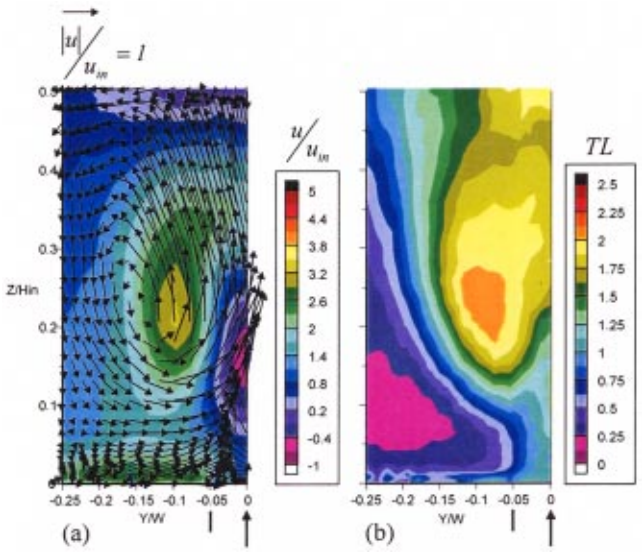

Fig. 8 Measured (*a*) secondary velocity vectors with contours of u/u_{in} and (*b*) turbulence levels for plane 1*p*

tween the two lobes as illustrated in Fig. 7 is quite large relative to that which would occur for a jet-in-cross-flow without an opposing jet.

At the dilution jet centerline, Fig. 7 illustrates the presence of film cooling near the wall even though there is only one row of cooling holes downstream of the dilution jets and upstream of this measurement plane. It is quite plausible that some of the upstream film-cooling flow has been wrapped around the dilution jet and is present at this location. It is also interesting to note the warmer temperatures that occur as one progresses up from the film-cooling layer to the dilution jet core at $Y/W=0$. The warmest fluid occurs at the same location as the highest negative streamwise velocity contour indicating a strong vortex motion, as will be discussed for Fig. 8.

Figure 8(*a*) shows the secondary velocity vectors (v and w) superimposed on the normalized streamwise velocity (u/u_{in}) contours in plane 1*p*. The measurement plane was taken across a symmetric section of the combustor simulator. There is a clear kidney-shaped vortex exhibited by the secondary velocity vectors as a result of the shear produced from the jet-mainstream interaction. The velocity contours indicate a strong backward streamwise velocity located at $Z/H_{in}=0.15$ at the hole centerline ($Y/W=0$). The contours indicate velocities as high as three times the inlet velocity near $Y/W=-0.075$ and $Z/H_{in}=0.2$. These high velocities do not coincide with the center of the vortex core. Near the spanwise center of the plane ($Z/H_{in}=0.5$), the streamwise velocity contours indicate a nearly stagnant region as a result of the interaction between the top and bottom dilution jets.

The turbulent flow field was also quantified for the cross-stream plane 1*p*, as shown in Fig. 8(*b*). The turbulence levels were calculated using all three velocity fluctuations and then normalized using the inlet velocity (u_{in}). The turbulence levels produced by the jet-mainstream interaction are incredibly high, particularly in the high-velocity region and at the mid-span region where the jets are impacting one another.

Downstream of the Second Row of Dilution Jets. The thermal field through the center of the second row of dilution jets is shown in Fig. 9 for plane 2*s*. The second row of dilution jets are injecting near the start of the contraction section of the combustor simulator. The momentum flux and mass flux ratios for these jets are somewhat lower than the first row at $I=32$ and $M=6$.

While the momentum flux ratio is much lower for the second row of dilution jets as compared to the first row, the physical penetration distance is not that different. In comparing the physical penetration distances of the $\theta=0.95$ contour in Figs. 6 and 9

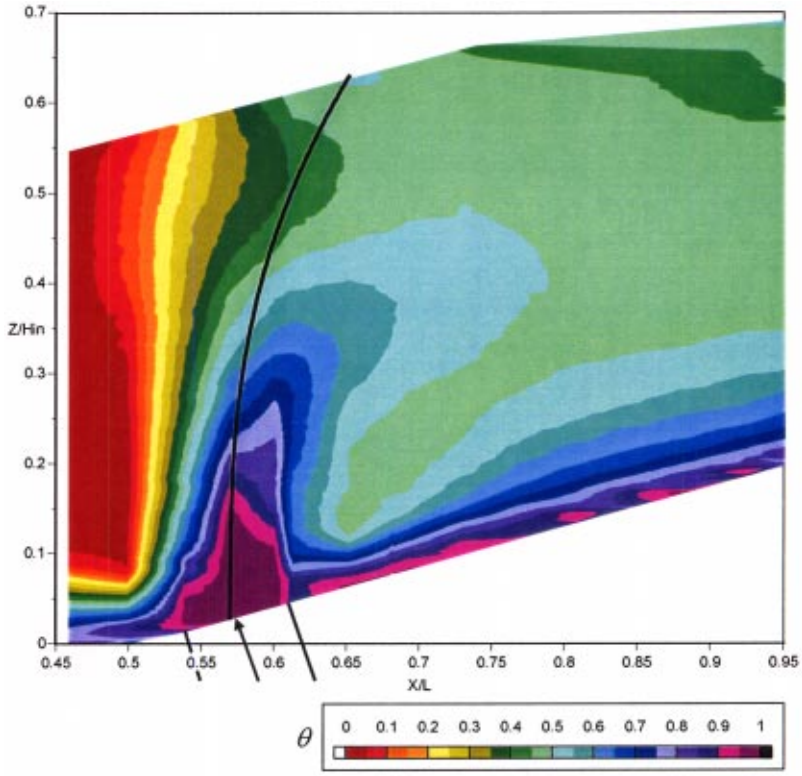

Fig. 9 Thermal field contours for plane 2*s* showing Lefebvre's [15] jet penetration correlation

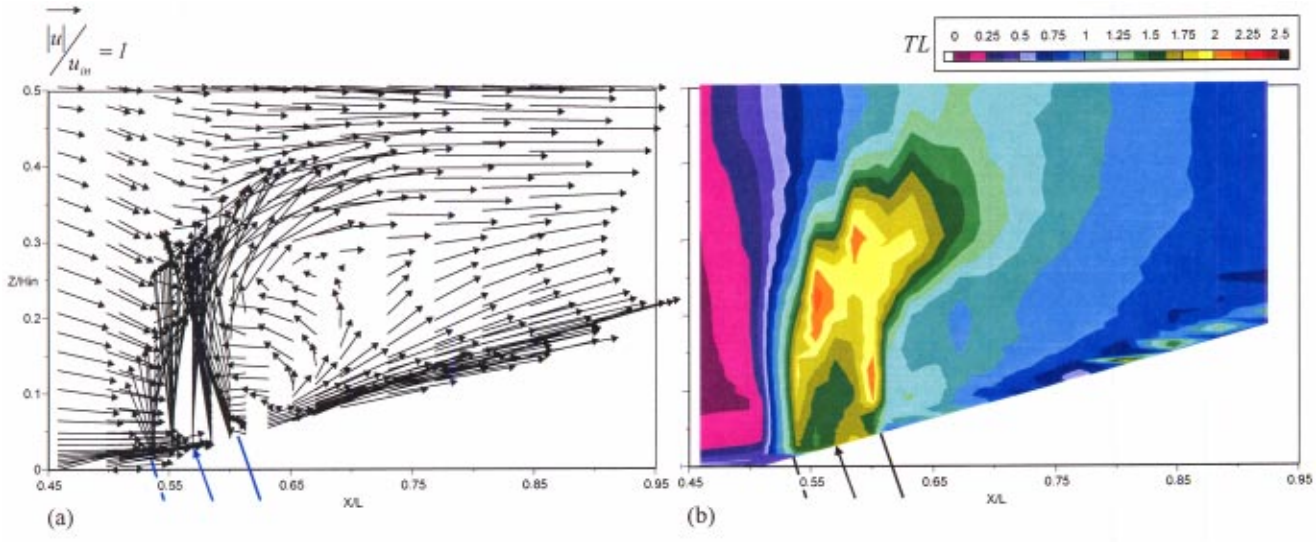

Fig. 10 (*a*), (*b*) Flow field vectors (left) and contours of turbulence levels (right) for plane 2*s*, downstream of the second row of dilution jets

for the two rows of dilution holes, the Z/H_{in} penetration depth for each is 0.1 and 0.12, respectively. In relating this distance to the respective hole diameters, however, there is a different answer. The first row of jets penetrated to a $Z/D_1=1.2$ while the second row of jets only penetrated only to $Z/D_2=0.95$. The solid line in Fig. 9 indicates the dilution jet trajectory predicted by Lefebvre's correlation [15]. As with the higher momentum dilution jets, the correlation predicts the trajectory of the dilution flow fairly accurately near the liner panels; however, the bending of the dilution flow is underpredicted as the jet penetration continues into the mainstream. It is worth mentioning that Lefebvre's correlation for this lower momentum dilution jet seems to fit better than it did for the higher momentum first row dilution jets.

Similar to that of the first row of holes, the thermal gradients reduce in magnitude at the jet-mainstream interface as one progresses farther from the wall. Figure 9 also indicates the presence of a cooler bulge near $X/L=0.65$ with a thermal contour level of $\theta=0.45$. This cooler region is a result of the lateral spreading of the cooler fluid from the first dilution row.

The thermal field contours for the near-wall fluid indicate a relatively thick layer upstream of the dilution jet. Just downstream of the dilution jets, however, the layer is much thinner but there is still coolant present. The coolant that is present near the wall downstream of the injection is there, despite the fact that there is some streamwise distance (one dilution hole diameter) between the dilution location and the film-cooling injection location. While the film-cooling layer near the wall is relatively thin just downstream of the dilution injection, this layer becomes relatively thick caused by the increased turbulence levels generated from the dilution jet-mainstream interaction.

Two-component LDV measurements were made for the streamwise plane 2*s* given the symmetric nature of this location (the v-component was nominally zero). The streamwise velocity vectors in Fig. 10(*a*) indicate a downward velocity as the flow approaches the dilution injection location. This downward velocity is thought to be the result of the mainstream flow being deflected away from the jet-to-jet impingement of the first row of dilution at the mid-span center. The velocity vectors indicate that most of the jet is exiting from the downstream portion of the dilution hole, but are pointed toward the upstream direction. This is consistent with the thermal field contours presented in Fig. 9. These high velocities have enough momentum to have a jet trajectory that is directed upstream.

Downstream of the jets, the velocity vectors indicate a very large recirculation region, which is characterized by warmer fluid behind the dilution jet. Near the wall, it is clear that there is also reversed flow just downstream of the jet. The coolant present near the wall may be in fact transported to this region from the downstream film-cooling holes, which is consistent with the thinner coolant layer. The closest film-cooling injection is located at $X=1D_2$ downstream on the dilution injection. Near $X/L=0.75$, which is slightly greater than two dilution hole diameters ($X=2D_2$) downstream of the jet injection, is the end of the recirculating region.

The vectors also indicate that the flow has been accelerated both in the near wall region, due to the film-cooling jets, and above the jet injection near the mid-span, due to the dilution jet blockage. As the flow exits the combustor, the streamwise profiles still have remnants of these faster regions.

Figure 10(*b*) shows the turbulent flow field measurements for

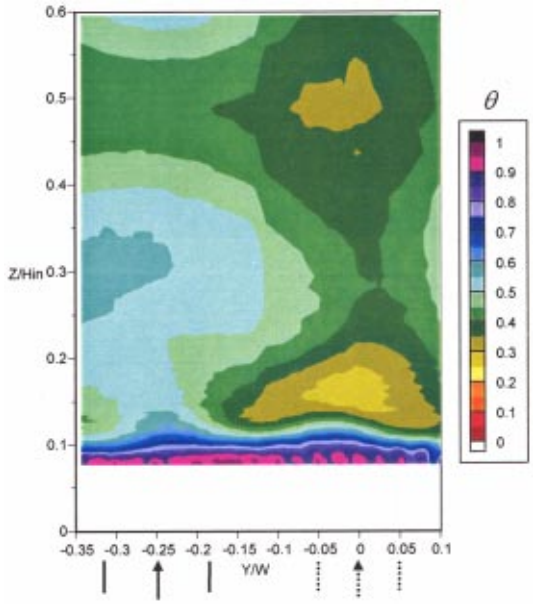

Fig. 11 Thermal field contours in plane 2*p* downstream of the second row of dilution

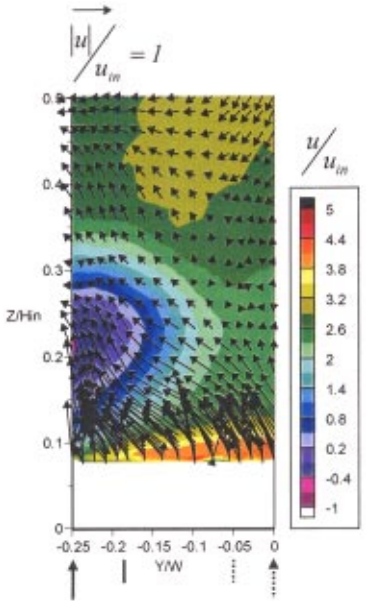

Fig. 12 Secondary velocity vectors with contours of the streamwise velocities in plane 2*p*

plane 2*s*. The peak turbulence levels, which occur at the jet-mainstream interface, are 2.2 times greater than the inlet velocity. It is important to recognize that at the dilution jet injection location, the mass-averaged velocity is 2.7 times that of the inlet velocity (indicated in Table 1) as a result of the mass flow injection from the first row of dilution jets and the film-cooling addition. The jet turbulence itself is relatively lower than that occurring as the jet interacts with the mainstream flow. In the jet recirculating region, the turbulence levels are very high, considering the fact that the local flow velocities in this region are relatively low. The near-wall turbulence that is generated is also relatively high due to the film-cooling injection. As the flow exits the combustor, the levels relative to the local exit velocity are on the order of 20%.

Figure 11 shows the thermal field contours downstream of the second row of dilution jets (plane 2*p*) for a region larger than the symmetric locations to illustrate the thermal field symmetry. Note that both jets inject to approximately the same spanwise location relative to the mid-span. The dashed lines represent the spanwise injection location of the first row of dilution holes while the solid lines represent the second row of dilution holes. At this streamwise location, which is one dilution hole diameter downstream of the second row of dilution holes ($X=1D_2$), the coldest temperature contour for the dilution flow is $\theta=0.55$ located at $Y/W=-0.25$ at about $Z/H_{in}=0.3$. The warmer fluid shown near $Y/W=0$ at $Z/H_{in}=0.15$ is a remnant of the warm fluid that is trapped in the recirculating region downstream of the first row of dilution jets. A similarly warm region is located just above that region near the mid-span, which is a result of warmer fluid penetrating between the opposing first row of dilution jets.

Figure 12 shows the secondary velocity vectors superimposed on the streamwise velocity contours at the same plane 2*p* only with a smaller measurement region as compared with Fig. 10. At this location, it is clear that there is no evidence from the vectors as to a strong kidney vortex as there was in the case of the first row of dilution holes. The high turbulence levels, as will be illustrated in the upcoming figures, have caused a reduction in the swirl velocities. There is a strong upward flow that is a result of the contraction section of the combustor. The streamwise velocities indicate that the flow has accelerated to about three times the inlet velocity near the mid-span. At a span of approximately 25% of the inlet height, there is a near zero velocity just downstream of the dilution holes, similar to that of the first row of dilution jets, which is caused by the jet blockage. To illustrate the anisotropic behavior of the turbulence of the dilution jets, Figs. 13(*a*)–13(*c*) show the measured fluctuations for all three velocity components. As can be seen, all three contour plots illustrate a very different behavior. The highest fluctuation levels in this plane are 1.75 times that of the inlet velocity. It is important to remember that at this location the mass-averaged velocity is 2.7 times faster than the inlet velocity, which still translates to average rms levels that

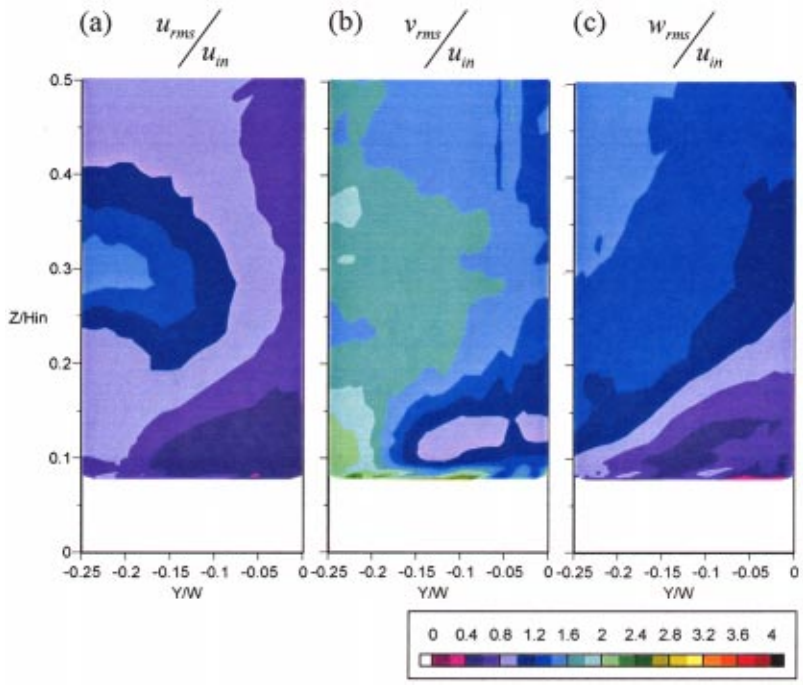

Fig. 13 (*a*)–(*c*) Contours of the rms fluctuations for the flow in plane 2*p*

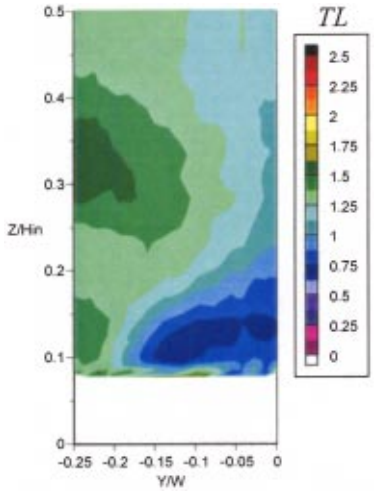

Fig. 14 Contours of turbulence levels in plane 2*p*

are 0.65 times the local mass averaged velocity. The peak streamwise velocity fluctuations occurs at $Z/H_{in}=0.3$ and $Y/W=-0.25$, which coincides with the core of the jet (as indicated by the thermal field contours in Fig. 11). The peak spanwise velocity fluctuations (v_{rms}), which are slightly higher at 2.1 times the inlet velocity, occur near the liner wall just below the core of the jet. Similar to the streamwise fluctuations, the peak spanwise fluctuations occur at the core of the jet and above.

The turbulence levels for the pitchwise plane, which is a combination of the fluctuations for all three velocity components, is shown in Fig. 14 for plane $2p$. For the second row of injection ($Y/W=-0.25$), the peak level coincides with a region slightly higher than the core of the jet. While the levels are much lower, the peak region for the first row of dilution jets coincides more closely with the mid-span.

Conclusions and Recommendations

The results of this study indicate the complexity of the flow that occurs in a typical aeroengine combustor. While these results were acquired with a nonreacting flow, it is important to have a place to begin when it comes to making comparisons with computational predictions. In particular, it is important that we are able to understand how the interactions take place between rows of dilution jets and liner film-cooling. The resolution of the measured data presented in this paper was only made possible through scaling up of a combustor.

The measurements indicate the dominance of the dilution jets on the flow and thermal fields. Kidney-shaped thermal fields were present as the result of the dilution jet-mainstream interaction. One notable feature was the spreading of the two kidney lobes that resulted from the impacting of the jets. Downstream of the dilution jet injection, there was a large recirculating region that transported warm fluid into the region just downstream of the injection. While the near-wall film of coolant is much thinner just downstream of the dilution holes, there is still coolant present. To determine whether the coolant was transported by vortices wrapping around the dilution jet or transported by the reverse flow downstream of the dilution jet is not known at this time. Further work needs to be conducted to determine the true mechanism that is important for combustor cooling strategies.

The turbulence levels were measured to be extremely high throughout the combustor as well as highly anisotropic. It is clear as to why current two-equation turbulence models underpredict these turbulence levels given the model assumptions of isotropic turbulence. The exit turbulence levels, based on the local average exit velocity were 20%.

Further studies need to be done to evaluate cooling schemes along the liner wall and ensure good coverage near the dilution holes. More detailed measurements are needed near the dilution holes to evaluate these cooling schemes. Given the results presented in this paper, it is possible to compare computational predictions with measured flow and thermal fields.

Acknowledgments

The authors gratefully acknowledge United Technologies—Pratt and Whitney for their support of this work.

Nomenclature

ALP = air loading parameter, $ALP=P_0^{1.75}A_{ref}D_{ref}^{0.75}e^{T/300}/\dot{m}$, Lefebvre [15]
d = film cooling hole diameter
D_1, D_2 = dilution hole diameters for first and second rows
H_{in} = combustor inlet height
I = momentum flux ratio, $I=\rho_c U_c^2/\rho_\infty U_\infty^2$
L = film cooling hole length, combustor simulator length
$\dot{m}$ = mass flow rate
M = mass flux ratio, $M=\rho_c U_c/\rho_\infty U_\infty$
P = vane pitch
S_s, S_p = streamwise, pitchwise film cooling hole spacing
T = temperature
TL = turbulence level, $TL=0.33(u_{rms}^2+v_{rms}^2+w_{rms}^2)^{0.5}/u_{in}$ (3-comp.) and $TL=0.5(u_{rms}^2+w_{rms}^2)^{0.5}/u_{in}$ (2-comp.)
u, v, w = local, mean velocity components
X, Y, Z = coordinate system shown in Fig. 2(a)
W = combustor inlet width

Greek

ρ = density
ν = kinematic viscosity
θ = nondimensional temperature, $\theta=(T_\infty-T)/(T_\infty-T_c)$

Subscripts

ave = spatial average
rms = root mean square
∞ = free-stream conditions (primary flow)
c = coolant conditions (secondary flow)

References

[1] Barringer, M. D., 2001, "Design and Benchmarking of a Combustor Simulator Relevant to Gas Turbine Engines," Master's thesis, Virginia Polytechnic Institute and State University.
[2] Zimmerman, D. R., 1979, "Laser Anemometer Measurements at the Exit of a T63-C20 Combustor," National Aeronautics and Space Administration, NASA Lewis Research Center, Contract No. NAS 3-21267.
[3] Goldstein, R. J., 1983, "Velocity and Turbulence Measurements in Combustion Systems," Exp. Fluids, **1**, pp. 93–99.
[4] Moss, R. W., 1992, "The Effects of Turbulence Length Scale on Heat Transfer," Ph.D. dissertation, Department of Engineering Science, University of Oxford, Report No. OUEL 1924/92.
[5] Cameron, C., Brouwer, J., Wood, C., and Samuelson, G., 1989, "A Detailed Characterization of the Velocity and Thermal Fields in a Model Can Combustor With Wall Jet Injection," ASME J. Eng. Gas Turbines Power, **111**, pp. 31–35.
[6] Gulati, A., Tolpadi, A., VanDuesen, G., and Burrus, D., 1995, "Effect of Dilution Air on the Scalar Flowfield at Combustor Sector Exit," J. Propul. Power, **11**, pp. 1162–1169.
[7] Holdeman, J. D., 1993, "Mixing of Multiple Jets With a Confined Subsonic Crossflow," Prog. Energy Combust. Sci., **19**, pp. 31–70.
[8] Stitzel, S. M., 2001, "Flow Field Computations of Combustor-Turbine Interaction in a Gas Turbine Engine," Master's thesis, Virginia Polytechnic Institute and State University.
[9] Malecki, R., Rhie, C., McKinney, R., Ouyang, H., Syed, S., Colket, M., and Madhabushi, R., 2001, "Application of an Advanced CFD-Based Analysis

System to the PW6000 Combustor to Optimize Exit Temperature Distribution—Part I: Description and Validation of the Analysis Tool,'' ASME Paper No. 2001-GT-0062.
[10] Goebel, S., Abauf, N., Lovett, J., and Lee, C., 1993, ''Measurements of Combustor Velocity and Turbulence Profiles,'' ASME Paper No. 93-GT-228.
[11] Stevens, S. J., and Carotte, J. F., 1990, ''Experimental Studies of Combustor Dilution Zone Aerodynamics, Part I: Mean Flowfields,'' J. Propul. Power, **6**, pp. 297–304.
[12] Liou, T. M., and Wu, Y. Y., 1992, ''LDV Measurements of the Flowfield in a Simulated Combustor With Axial and Side Inlets,'' Exp. Therm. Fluid Sci., **5**, pp. 401–409.
[13] Barringer, M. D., Richard, O. T., Walter, J. P., Stitzel, S. M., and Thole, K. A., 2001, ''Flow Field Simulations of a Gas Turbine Combustor,'' ASME J. Turbomach., **124**, pp. 508–516.
[14] Moffat, J. R., 1988, ''Describing the Uncertainties in Experimental Results,'' Exp. Therm. Fluid Sci., **1**, pp. 3–17.
[15] Lefebvre, A. H., 1999, *Gas Turbine Combustion*, Taylor & Francis, Philadelphia, PA.